Int Urogynecol J (2016) 27:205–212
DOI 10.1007/s00192-015-2804-8

ORIGINAL ARTICLE

Assessment of urethral support using MRI-derived computational modeling of the female pelvis

Yun Peng[1] · Rose Khavari[2] · Nissrine A. Nakib[3] · Timothy B. Boone[2] · Yingchun Zhang[1]

Received: 18 April 2015 / Accepted: 13 July 2015 / Published online: 30 July 2015

Abstract
Introduction and hypothesis This study aimed to assess the role of individual anatomical structures and their combinations to urethral support function.
Methods A realistic pelvic model was developed from an asymptomatic female patient's magnetic resonance (MR) images for dynamic biomechanical analysis using the finite element method. Validation was performed by comparing simulation results with dynamic MR imaging observations. Weaknesses of anatomical support structures were simulated by reducing their material stiffness. Urethral mobility was quantified by examining urethral axis excursion from rest to the final state (intra-abdominal pressure=100 cmH_2O). Seven individual support structures and five of their combinations were studied.
Result Among seven urethral support structures, we found that weakening the vaginal walls, puborectalis muscle, and pubococcygeus muscle generated the top three largest urethral excursion angles. A linear relationship was found between urethral axis excursions and intra-abdominal pressure. Weakening all three levator ani components together caused a larger weakening effect than the sum of each individually weakened component, indicating a nonlinearly additive pattern. The pelvic floor responded to different weakening conditions distinctly: weakening the vaginal wall developed urethral mobility through the collapsed vaginal canal, while weakening the levator ani showed a more uniform pelvic floor deformation.
Conclusions The computational modeling and dynamic biomechanical analysis provides a powerful tool to better understand the dynamics of the female pelvis under pressure events. The vaginal walls, puborectalis, and pubococcygeus are the most important individual structures in providing urethral support. The levator ani muscle group provides urethral support in a well-coordinated way with a nonlinearly additive pattern.

Keywords Stress urinary incontinence · Magnetic resonance imaging · Pelvic muscle · Urethral hypermobility · Finite element method

Introduction

Lack of urethral support due to weakness in various components of the urethral support system (USS) has been considered as the main etiological factor causing stress urinary incontinence (SUI) [1]. The "hammock hypothesis" describes support of the urethra by a coordinated action of fasciae and muscles, which provides a hammock onto which the urethra is compressed during increases in intra-abdominal pressure (IAP) [1]. In a broad sense, the USS includes the levator ani muscle, vaginal wall, and connective tissues extrinsic to the urethra, as well as the coccygeus muscle, obturator internus muscle, piriformis muscle, and pelvic organs such as the rectum and uterus, as all these structures reside in the female pelvis and interact intimately to support the urethra during pressure events.

Many studies have investigated the pathophysiology of SUI through medical imaging techniques such as

✉ Yingchun Zhang
yzhang94@uh.edu

[1] Department of Biomedical Engineering, Cullen College of Engineering, University of Houston, 2027 SERC Building, 3605 Cullen Blvd, Houston, TX 77024, USA

[2] Department of Urology, Houston Methodist Hospital and Research Institute, Houston, TX 77030, USA

[3] Department of Urology, University of Minnesota, Minneapolis, MN, USA

ultrasonography (US) [2], anatomical magnetic resonance (MR) imaging [3], and dynamic MR imaging [4]. To assess urethral hypermobility caused by isolated impairment of each specific USS component and to compare components' relative contribution to urethral support function would require the recruitment of patients with only one impairment condition, which is clinically challenging to identify. Cross-subject differences in female pelvic floor anatomy also affect the objectivity of the comparison. Computer modeling using MR images and simulation using the finite element method (FEM) has proven to be a useful tool [5, 6] due to its ability to conveniently simulate various impairment conditions and keep these comparisons based on the same patient [7, 8]. Several computer models developed from MR images have been reported recently in studies of female pelvic floor dysfunctions, such as pelvic organ prolapse (POP) [9–11], childbirth-related levator ani muscle damage [12], and ligament impairment [13]. However, the clinical application of these models and their comparisons with the true dynamic response of the pelvis is limited due to either (1) missed or simplified important anatomical structures (e.g., bladder, rectum, vaginal canal, uterus are not imaged [12] or buffering fatty tissues are not included [9–13]); or (2) less accurate imaging of boundary conditions (e.g., direct inferior displacement is applied on the uterus [9]; intra-abdominal pressure (IAP) is directly applied on the muscle [13] or vaginal wall [11]). A comprehensive pelvic model incorporating 44 anatomical structures that maintain integrity of the natural female pelvic anatomy was developed in this study to better understand the role of individual structures and their combinations on urethral support in women.

Materials and methods

A 21-year-old healthy woman [nulliparous, nonsmoker, body mass index (BMI)=22] was recruited according to a protocol approved by the Institutional Review Boards (IRBs) of the University of Minnesota and the University of Houston to undergo a high-resolution pelvic scan in the supine position at rest with a 3T MR imaging scanner (Trio Tim, Siemens, Germany) (slice thickness 3 mm; matrix 320×160; field of view 430 mm; pixel size 1.344 mm). For validation purposes, dynamic MR images were acquired in the midsagittal plane approximately every 1.5 s while the patient performed several Valsalva maneuvers.

Image segmentation was first performed on axial images for each anatomical pelvic structure with the guidance of urologists using Mimics 11.0 (Materialise Group, Leuven, Belgium). The closed surfaces were reconstructed for each anatomical structure and exported in stereolithography (STL) format. Those surfaces were imported into MAYA 8.5 (Autodesk, Inc., San Rafael, CA, USA) and Rhinoceros 4.0 (McNeel North America, Seattle, WA, USA) for artifact smoothing and intersecting surface correction and then converted into solid Standard ACIS Text (SAT) geometries. All solid geometries were discretized into finite element meshes with a total number of 126,378 tetrahedral elements in ABAQUS 6.12 (SIMULIA, Providence, RI, USA). The final 3D pelvic model contains 44 anatomical parts, including pelvic muscles, sphincteric muscles, ligaments, bones, fat, bladder, urethra, uterus, vagina, deep perineal pouch, colon, rectum, and anus. In addition, a bodyfill part was created to fill the intra-abdominal space for pressure transmission. A stiff Q-tip swab part was placed in the urethra to simulate the Q-tip swab that has been frequently used in clinical diagnosis and research for SUI [14, 15]. Figure 1 illustrates the reconstructed 3D pelvic model. The bottom of the model was restrained from both translations and rotations. Two uniformly distributed pressures were applied on the front and top surfaces of the bodyfill to simulate Valsalva. IAP was calculated as the averaged contact pressure between the urine and inner bladder wall.

Although soft tissues show viscoelastic behavior [16–18], a previous study found quasi-linear material property of urological soft tissues when the stress level is under 70 % of the maximal stress value [8]. Soft tissues involved in the pelvic model were modeled as linear elastic solids using material properties from Young's moduli of the bladder, urethra, uterus, rectum, muscle, ligament, and vaginal tissue (0.05, 0.03, 0.05, 0.1, 2.4, 1.2, and 7.4e–3 MPa) [7]. A soft material (Young's modulus of 0.04 MPa) was assigned to the bodyfill part. Urine was modeled as an elastic liquid with a Young's modulus of 1.0e–3 MPa. All soft tissues were considered incompressible considering that they contain abundant water. The bony pelvis was modeled as one rigid and fixed structure considering its negligible deformation under normal pelvic functions due to its much higher stiffness compared with soft tissues [13]. A simplifying condition was created so as to not include voluntary contraction of the pelvic muscles, as it is often the case that, unless the patient is trained to use pelvic floor physical therapy, the pelvic floor responds to acute increase of IAP without voluntary contractions, such as during coughing or sneezing.

The general contact algorithm in ABAQUS was applied to mimic the natural interaction between parts that are in contact but anatomically independent, such as bladder and uterus, uterus and rectum, or pelvic muscles and fatty tissues. Tie constraints in ABAQUS that binds two shared surfaces were used to couple motions of parts that are biologically connected (e.g., coccygeus muscle and coccyx) and to model the connecting effects of fasciae (e.g., tendineus arch of levator ani muscle between iliococcygeus muscle and obturator internus muscle). Connector elements, with the ability to model connective tissues such ligaments [9], were employed to model uterosacral and cardinal ligaments. The Abaqus/Explicit solver was used for finite-element-method implementation.

A validation study was first performed by comparing pelvic floor configurations achieved in computer simulation results

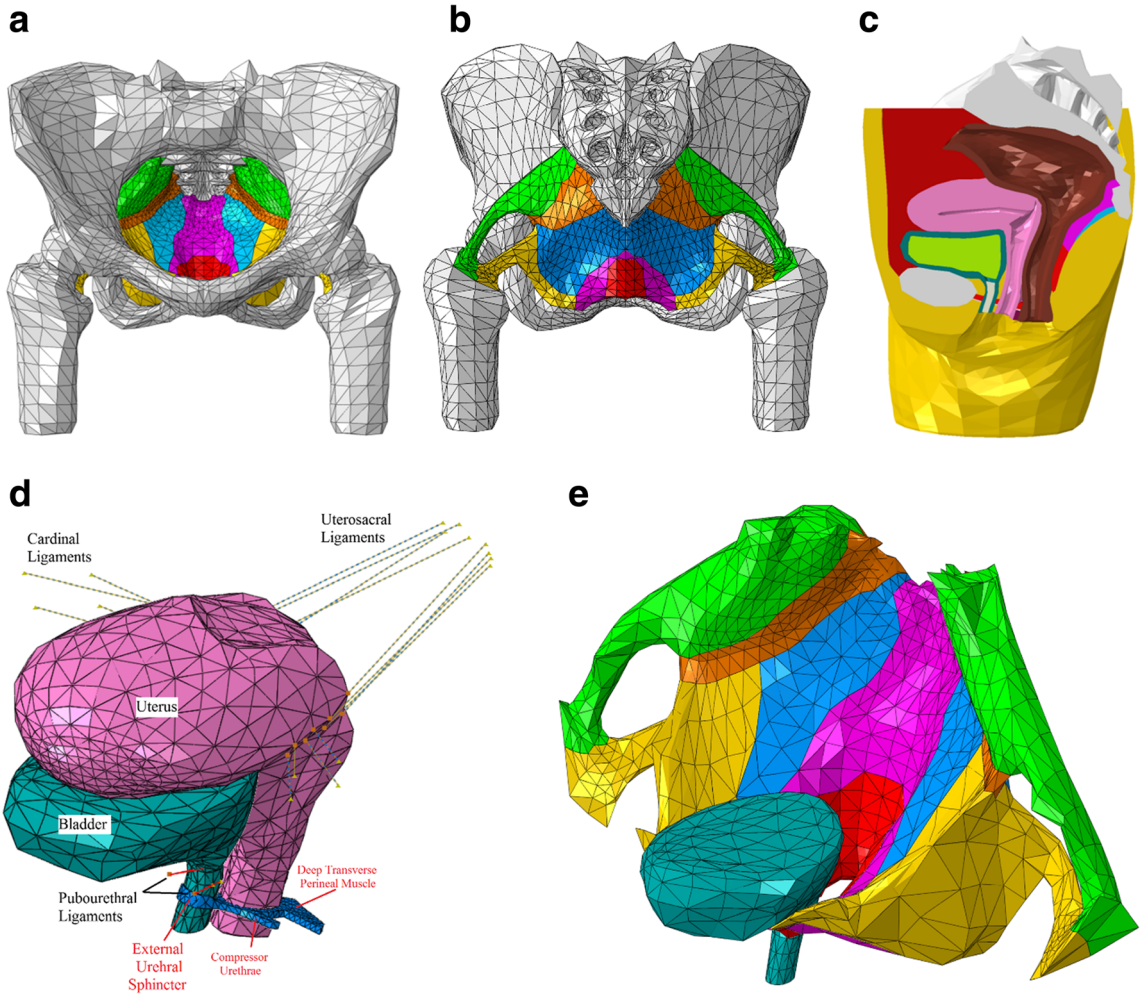

Fig. 1 **a** Front and **b** back view of all pelvic muscles, ligaments, and bones (fats and organs hidden for better visualization). **c** Midsagittal view of the entire pelvic model. **d** Anterior and posterior supports to urethra from pubourethral ligament, vagina, and perineal pouch muscles. Ligaments were modeled using connector elements. The uterosacral ligaments attach the cervix to the posterior pelvic wall. The cardinal ligaments attach the cervix to the lateral pelvic wall. The pubourethral ligaments attach the bladder neck to the symphysis pubis. **e** Posterior support to urethra from pelvic floor muscles. In **a**, **b**, and **e**, muscles are shown in different colors (*green* piriformis, *orange* coccygeus, *blue* iliococcygeus, *yellow* obturator internus, *magenta* pubococcygeus, *red* puborectalis)

with dynamic MR imaging observations along the midsagittal plane at both rest and maximal Valsalva maneuver (Fig. 2). The patient was instructed on how to perform a Valsalva maneuver for the dynamic MR imaging and asked to hold each Valsalva maneuver for at least 2 s. During Valsalva maneuver, abdominal muscles were contracted. Special attention was paid to motions of the bladder, urethra, uterus, and rectum. Results showed that the bladder, uterus, and rectum slide in a posterior direction under the elevated IAP. It was also observed that the increased IAP led to bladder-neck descent and clockwise rotation of the urethra, both of which are important landmarks commonly used in assessing urethral supports. The achieved consistency demonstrated the competence of the computer modeling and simulation method in characterizing pelvic floor responses to increased IAP.

The plan of simulation used in this study is listed in Table 1. The first two columns list the test numbers and weakened parts, with their abbreviations in brackets. The impairment of each structure was simulated by reducing the material stiffness by 90 % [13]. Test00 serves as the asymptomatic control test based on the intact model in which no impairment was present. In each test from 01 to 07, a single USS component was weakened (hereafter referred to as single tests); in each test from 08 to 12, a specific group of USS components was weakened (hereafter referred to as group tests). Weakening the levator ani muscle was considered as a group test because the levator ani muscle group is composed of three individual muscle components. SUI is often associated with urethral hypermobility. Transperineal US reveals that the alpha-angle, defined as the angle between the vertical axis and the urethral axis [2], was significantly different on straining ($P<0.05$) between the study (SUI) and control groups. In this study, the alpha angle was monitored from the onset of simulation to the final status, at which the IAP reached 100 cmH_2O [19]. The

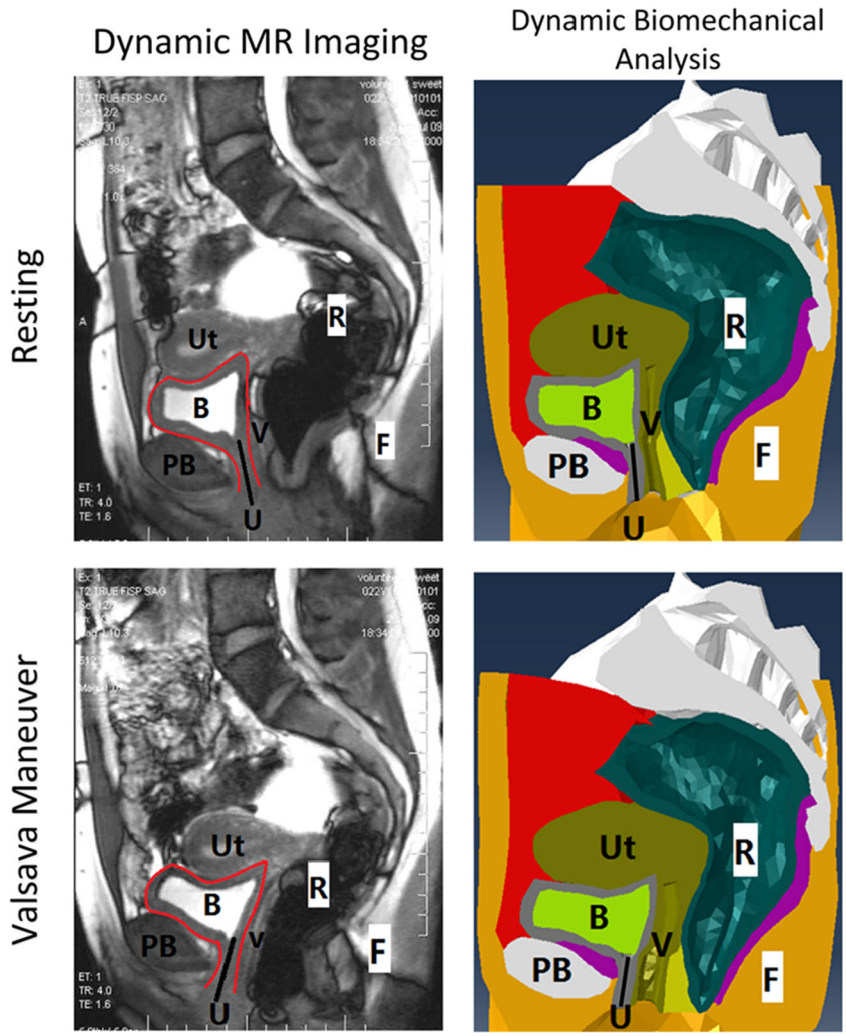

Fig. 2 Comparison [dynamic magnetic resonance (MR) imaging vs. dynamic biomechanical analysis] in the sagittal plane of pelvic structures of the female patient at rest and on Valsalva. The *black solid line* in all images shows the location of the urethra. The *red curves* in the dynamic MR image outline the bladder. *Ut* uterus, *R* rectum, *B* bladder, *PB* pubic bone, *V* vagina, *F* fat, *U* urethra)

urethral excursion angle, defined by the corresponding change in the α angle ($\Delta\alpha$) and mathematically equal to the Q-tip excursion in clinical tests [15], was also monitored as an alternative metric to examine the urethral support function. Since the α angle at rest showed no significant difference (P=0.650) between SUI and control groups [2], and because only urethral support loss attributed to weakness of specific anatomical structure(s) was considered in this computation study, static morphologic variation in the α angle between asymptomatic individuals and patients with SUI was not accounted for.

Linear regression analyses were performed for all curves (urethral excursion angles vs. IAP) in MATLAB R2014 (Mathworks Inc., Natick, MA, USA) using a linear model ($\Delta\alpha \sim k \times IAP$). The interception of the linear model was set to zero, considering that the urethral excursion angle should be zero at the onset of simulation (IAP=0 cmH_2O). The $\Delta\alpha$ achieved in the intact test (noted as $\Delta\alpha_{Intact}$) indicates the inherent response to the applied IAP of an asymptomatic USS. A weakening effect index (WEI)($\Delta\alpha - \Delta\alpha_{Intact}$) was also employed to elicit the degree of mobility caused solely by the weakened structure in each weakening test.

Results

The α angle at onset of simulation (at rest) was 15.9° for all tests. Table 1 shows the α angles achieved at the final status with the IAP of 100 cmH_2O for all tests. The final α angles ranged from 30.3° (intact test) to 50.7° (weakened levator ani muscle and vaginal wall). The corresponding urethral excursion angles ($\Delta\alpha$) were calculated based on the difference between onset and final α angles (Table 1); $\Delta\alpha_{Intact}$ reached 14.4° for the particular participant in this study. The results further showed that $\Delta\alpha$ values were <20° when only a single pelvic muscle was weakened (from 15.3° to 19.4°). The vaginal wall, the puborectalis muscle, and the pubococcygeus muscle were found to be the top three most contributing structures. Weakening these parts generated the top three largest urethral excursion angles ($\Delta\alpha$=20.1°, 19.4°, and 18.8°,

Table 1 Simulation plan and results

Test no.	Weakened part (abbreviation)	α angle (°) at IAP=100 cmH_2O	Q-tip excursion $\Delta\alpha$ (°)	Weakening effect index (WEI)=$\Delta\alpha-\Delta\alpha_{intact}$ (°)
00	None	30.3	14.4 ($\Delta\alpha_{Intact}$)	0.0
Single tests				
01	Coccygeus Muscle (CM)	31.1	15.3	0.8
02	Iliococcygeus Muscle (ICM)	31.6	15.8	1.4
03	Piriformis Muscle (PM)	32.2	16.3	1.9
04	Obturator Internus Muscle (OIM)	31.5	15.6	1.2
05	Puborectalis Muscle (PRM)	35.3	19.4	5.0
06	Pubococcygeus Muscle (PCM)	34.7	18.8	4.4
07	Vaginal Wall (VW)	36.0	20.1	5.7
Group tests				
08	PRM + PCM	42.2	26.4	12.0
09	PRM+PCM+ICM = Levator Ani Muscle (LAM)	48.8	32.9	18.5
10	LAM + CM	49.0	33.2	18.8
11	LAM + OIM	50.0	34.1	19.7
12	LAM + VW	50.7	34.9	20.4

α angle=15.9° at rest for all tests

respectively), while weakening other muscles (the iliococcygeus, piriformis, coccygeus, and obturator internus muscles) generated relatively smaller excursion angles ($\Delta\alpha$ <17°). Weakening the levator ani muscle alone (test09) or in combination with other pelvic muscles (test10–12) raised the $\Delta\alpha$ value >30°. The fitted R-square values for the urethral excursion angle–IAP curves (see Fig. 3) fell into the range of 0.95–0.99, indicating a strong linear relationship between the urethral excursion angle and increased IAP for all tests.

A nonlinearly additive pattern was found among the three levator ani muscle components in terms of weakening effect (WEI=$\Delta\alpha-\Delta\alpha_{Intact}$). A WEI of 12.0° was achieved when weakening the puborectalis and pubococcygeus muscles together (test08), which is larger than the sum of WEI achieved by weakening these two muscles separately (WEI=5.0° in test05; WEI=4.4° in test06). The same nonlinear additive pattern was more remarkable when comparing the WEI obtained from weakening the entire levator ani muscle (WEI=18.5°, test09) with the sum of WEIs from tests in weakening the three components separately (WEI=1.4° in test02, WEI=5.0° in test05, WEI=4.4° in test06). Such a pattern did not exist for combinations of the levator ani muscle with other muscle groups (test10, 11, 12). This finding suggests that the levator ani muscle is a sophisticated structure that provides support to the urethra in a well-coordinated fashion.

Distinct deformation patterns were found in pelvic floor responses under different weakening conditions (see Fig. 4). When vaginal tissues were weakened, the vaginal canal underwent severe compression and the vaginal wall became extremely thin, yielding more space for extraurethral motion; however, the shape and position of the levator ani muscle did not show evident difference. When the levator ani muscle was weakened, a different pattern was observed: the vaginal wall remained at its normal thickness, while the levator ani muscle showed remarkable backward and downward yielding, especially in the midportion, as the combinational effect of the front and top pressures applied on the bodyfill part on the entire pelvic floor was similar to a body force oriented in the inferoposterior direction and perpendicular to the levator plate. Urethral-axis excursion in this case was attributed more to insufficient support by the weakened levator ani muscle than the collapsed vaginal canal. When the levator ani muscle and the vaginal wall were both weakened simultaneously, both syndromes could be identified.

Discussion

Our female pelvic model consisting of 44 anatomical structures to mimic the dynamic response to pressure events represents, to the best of our knowledge, the most comprehensive and complete pelvic model in female SUI research. The validation study demonstrated consistency between computer-simulation results and dynamic MR imaging observations along the sagittal plane of the pelvis of the same patient. A parametric study was designed and performed to investigate the relative importance of individual structures or their combination on urethral support in women. The α angles from our computer simulations are in agreement with findings from transperineal US [2].

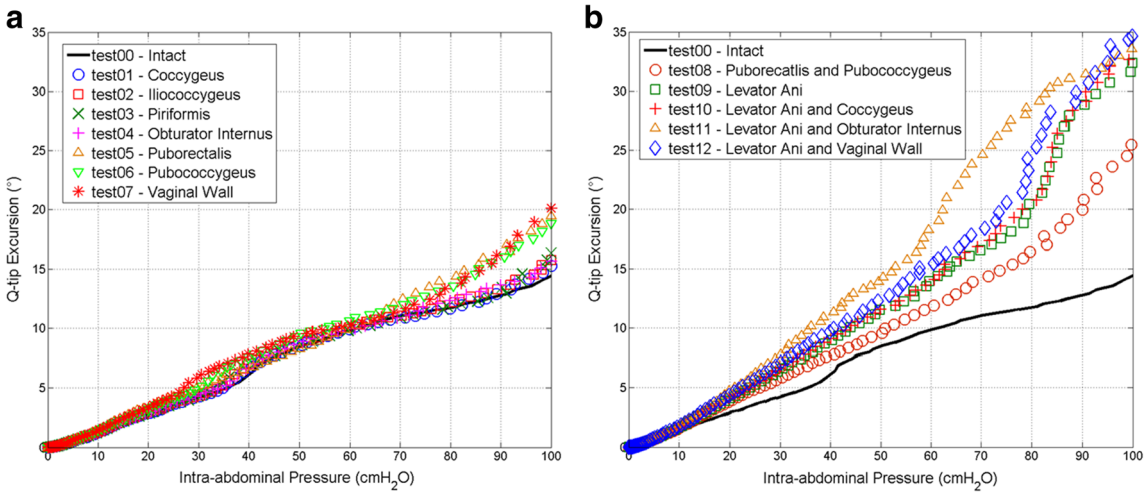

Fig. 3 Plots of urethral excursion angle against intra-abdominal pressure for **a** single and **b** group tests

The relationship between IAP and induced urethral hypermobility may vary widely across individuals due to differences in anatomy and functional status of the urethral support system [20]. However, simultaneous examination of these two metrics may provide useful information for standardized evaluation of the functional status of the female pelvis. A significant association (p=0.012) between the ratio of IAP over Q-tip angle (urethral mobility index) and the degree of cystourethrocele was reported in a study that involved 84 incontinence women [21]. The authors proposed this urethral mobility index as a standardized index for crossing-subject comparison. Although it is often intuitively assumed that the extent of urethral hypermobility should be positively related to IAP, this is the first time that this relationship has shown to be linear. The linear relationship over the entire IAP range identified in this study provided substantial ground for the application of the urethral mobility index, which could be obtained consistently at any IAP level with less vulnerability to IAP variations. Moreover, it could provide a comprehensive functional profile of the female pelvic floor in order to discern urethral mobility indices specific to each weakening condition. Any anatomical (such as midurethral sling surgery) or functional (e.g., enhanced pelvic muscle strength) change in the pelvis could also be simulated in the computational model to provide valuable references in presurgery planning, training, or other SUI treatment options.

In our model, the weakening effect was mild when only one single structure was weakened, consistent with Crystle et al., who found patients with good urethral support to have a rotation angle <20° [14]. This finding reveals that the female USS is a stable system and could still provide sufficient support to the urethra under mild impairment. Considering the Q-tip excursion >30° as a criteria for urethral hypermobility [14, 15], we find that weakening the entire levator ani muscle (comprised of the iliococcygeus, puborectalis and pubococcygeus muscles) caused more urethral mobility and could possibly result in urethral hypermobility ($\Delta\alpha$=32.9°). This is consistent with the clinical observation that female SUI patients with urethral hypermobility are often associated with damage to the levator ani muscle [22].

Medical imaging techniques such as MR imaging or US have been widely used for diagnosing SUI characterized by urethral hypermobility, but their application is limited to cases in which morphologic defects of urethral support structures are main causes. However, impairment is not always morphologically observable. Reduced stiffness in pelvic muscles [23] and ligament and vaginal wall tissues due to aging or trauma [24] could also be associated with insufficient support. The

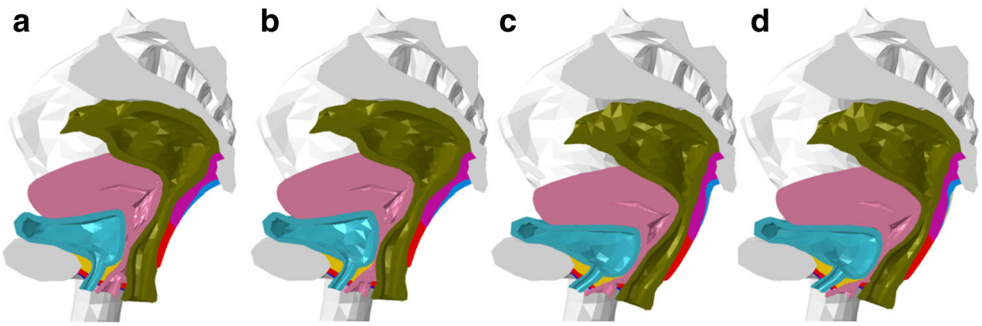

Fig. 4 Deformation patterns of **a** intact test, **b** weakened vaginal wall, **c** weakened levator ani muscle, and **d** weakened levator ani muscle together with vaginal wall

computational modeling and biomechanical approach provides a useful tool for those cases in which there is no imaging evidence of morphologic abnormalities in the USS. Moreover, with the capability to reproduce the pelvic floor deformation under different weakening scenarios, and exporting dynamic or static landmarks of interest, our model could be employed to establish a patient-specific SUI profile that manifests the deformation pattern uniquely associated with each possible weakening scenario. The functional status of the urethral support structure could then be assessed by comparing the imaging finding with the established profile. The distinct deformation patterns under different weakening conditions provide valuable references for patient-specific SUI diagnosis, which would be difficult to obtain from other methods considering the particularly challenging requirement that the same patient must develop different weakening syndromes successively, as well as the difficulty in capturing the extremely instantaneous dynamic deformation.

The computational modeling and biomechanical analysis approach presented in this study could also be employed to develop, design, and optimize interventional treatment approaches/devices, such as midurethral slings. Results under different weakening conditions provided in our model could be valuable in simulating worst-case scenarios and determining the safety factor for sling products. Kociszewski et al. [25] showed that success and complication rates of sling surgery were highly associated with implant position. Our model could also be used as a presurgery planning tool to reduce potential postoperative complications and improve treatment success rate on a patient-specific basis.

Limitations of this study are first, it lacks statistical information, as our model was built based on one patient-specific anatomy. The patient-specific-modeling approach provides a tool for personalized diagnosis and treatment outcome prediction for a specific patient. Analyses will be performed in the future based on results from a group of patients in order to provide statistical information. Second, the pelvic model relies on high-resolution MR images, which remains a relatively expensive procedure (approximately US $500/MR scan). Third, the modeling procedure takes about 1–2 weeks for experienced engineers and radiologists. A possible solution to make this approach more accessible is to build a pelvic model template based on features of the patient group and use patient-specific US images for model modification. Fourth, a limitation commonly shared by many other pelvic models is that the voluntary contraction of muscles is not possible in the pelvic model. To do so it would require a nontrivial finite element implementation technique as well as critical physiological calibrations for different levels of voluntary pelvic floor muscle contractions. Very recently, an advanced voluntary pelvic model was proposed that provides a way to model voluntary muscle contractions [26]. Nevertheless, the parameters associated with the voluntary muscle model were not obtained from actual voluntary contraction experiments in this study. A specially designed transvaginal and a transrectal high-density surface electromyogram (EMG) probe [27], along with the internal muscle activity imaging technique [28–30], were recently developed in our group. We are currently using high-density surface EMG measurements to quantitatively characterize voluntary muscle contractions in the female pelvis to further improve our pelvic modeling approach.

In conclusion, a comprehensive computational model of the female pelvis was reconstructed. The vaginal wall, puborectalis muscle, and pubococcygeus muscle were found to be the three most important urethral support structures. Some unique patterns of female pelvic floor deformation were identified, which indicate that the computational modeling and dynamic biomechanical analysis approach presents a powerful tool for female SUI research and clinical diagnosis. It could be potentially employed for patient-specific SUI evaluation and presurgery planning.

Acknowledgments This work was supported in part by NIH 4R00DK082644, NIH K99DK082644 and the University of Houston. The authors thank Dr. John O. DeLancey from the University of Michigan for his valuable consultation and Mr. Thomas Potter for editing the manuscript.

Conflicts of interest None.

References

1. Delancey JOL (1994) Structural support of the urethra as it relates to stress urinary-incontinence—the hammock hypothesis. Am J Obstet Gynecol 170(6):1713–1723
2. Sendag F, Vidinli H, Kazandi M, Itil IM, Askar N, Vidinli B, Pourbagher A (2003) Role of perineal sonography in the evaluation of patients with stress urinary incontinence. Aust N Z J Obstet Gynaecol 43(1):54–57
3. Heilbrun ME, Nygaard IE, Lockhart ME, Richter HE, Brown MB, Kenton KS, Rahn DD, Thomas JV, Weidner AC, Nager CW (2010) Correlation between levator ani muscle injuries on magnetic resonance imaging and fecal incontinence, pelvic organ prolapse, and urinary incontinence in primiparous women. Am J Obstet Gynecol 202(5):488. e481–488. e486
4. Del Vescovo R, Piccolo CL, Della Vecchia N, Giurazza F, Cazzato RL, Grasso RF, Zobel BB (2014) MRI role in morphological and functional assessment of the levator ani muscle: use in patients affected by stress urinary incontinence (SUI) before and after pelvic floor rehabilitation. Eur J Radiol 83(3):479–486. doi:10.1016/j.ejrad.2013.11.021
5. Peng Y, Dai Z, Mansy HA, Sandler RH, Balk RA, Royston TJ (2014) Sound transmission in the chest under surface excitation: an experimental and computational study with diagnostic applications. Med Biol Eng Comput 52(8):695–706
6. Wang S, Zhou Y, Tan J, Xu J, Yang J, Liu Y (2014) Computational modeling of magnetic nanoparticle targeting to stent surface under high gradient field. Comput Mech 53(3):403–412
7. Peng Y, Khavari R, Nakib NA, Stewart JN, Boone TB, Zhang Y (2015) The single-incision sling to treat female stress urinary

incontinence: a dynamic computational study of outcomes and risk factors. J Biomech Eng 137(9):091007
8. Zhang Y, Kim S, Erdman AG, Roberts KP, Timm GW (2009) Feasibility of using a computer modeling approach to study SUI induced by landing a jump. Ann Biomed Eng 37(7):1425–1433
9. Luo J, Chen L, Fenner DE, Ashton-Miller JA, DeLancey JOL (2015) A multi-compartment 3-D finite element model of rectocele and its interaction with cystocele. J Biomech 48(9):1580–1586
10. Ren S, Xie B, Wang J, Rong Q (2015) Three-dimensional modeling of the pelvic floor support systems of subjects with and without pelvic organ prolapse. BioMed Res Int 2015
11. Chen Z-W, Joli P, Feng Z-Q, Rahim M, Pirró N, Bellemare M-E (2015) Female patient-specific finite element modeling of pelvic organ prolapse (POP). J Biomech 48(2):238–245
12. Jing D, Ashton-Miller JA, DeLancey JO (2012) A subject-specific anisotropic visco-hyperelastic finite element model of female pelvic floor stress and strain during the second stage of labor. J Biomech 45(3):455–460
13. Brandão S, Parente M, Mascarenhas T, da Silva ARG, Ramos I, Jorge RN (2015) Biomechanical study on the bladder neck and urethral positions: simulation of impairment of the pelvic ligaments. J Biomech 48(2):217–223. doi:10.1016/j.jbiomech.2014.11.045
14. Crystle CD, Charme LS, Copeland WE (1971) Q-tip test in stress urinary incontinence. Obstet Gynecol 38(2):313
15. Ghoniem G, Stanford E, Kenton K, Achtari C, Goldberg R, Mascarenhas T, Parekh M, Tamussino K, Tosson S, Lose G (2008) Evaluation and outcome measures in the treatment of female urinary stress incontinence: International Urogynecological Association (IUGA) guidelines for research and clinical practice. Int Urogynecol J 19(1):5–33
16. Wang Q, Zeng H, Best TM, Haas C, Heffner NT, Agarwal S, Zhao Y (2014) A mechatronic system for quantitative application and assessment of massage-like actions in small animals. Ann Biomed Eng 42(1):36–49
17. Dai Z, Peng Y, Mansy HA, Sandler RH, Royston TJ (2014) Comparison of poroviscoelastic models for sound and vibration in the lungs. J Vib Acoust 136(5):050905
18. Zhou D, Peng Y, Bai J, Rosandich RG (2014) Contact effect evaluation using stress distribution in viscoelastic material under generalized loading. Int J Model Simul 34 (4)
19. Cobb WS, Burns JM, Kercher KW, Matthews BD, Norton HJ, Heniford BT (2005) Normal intraabdominal pressure in healthy adults. J Surg Res 129(2):231–235
20. Brandt FT, Lorenzato FR, Nobrega LV, Albuquerque CD, Falcao R, Araujo Junior AA (2006) Intra-abdominal pressure measurement during ultrasound assessment of women with stress urinary incontinence: a novel model. Acta Cir Bras Soc Bras Desenvolvimento Pesqui Cir 21(4):237–241
21. Alafraa T, Schick E (2008) Relation between Intra-abdominal pressure variation and urethral hypermobility: the urethral mobility index. Poster Abstract at International Continence Society
22. DeLancey JOL (2002) Fascial and muscular abnormalities in women with urethral hypermobility and anterior vaginal wall prolapse. Am J Obstet Gynecol 187(1):93–98. doi:10.1067/mob.2002.125733
23. Verelst M, Leivseth G (2007) Force and stiffness of the pelvic floor as function of muscle length: a comparison between women with and without stress urinary incontinence. Neurourol Urodyn 26(6):852–857
24. Chantereau P, Brieu M, Kammal M, Farthmann J, Gabriel B, Cosson M (2014) Mechanical properties of pelvic soft tissue of young women and impact of aging. Int Urogynecol J 25(11):1547–1553
25. Kociszewski J, Rautenberg O, Kolben S, Eberhard J, Hilgers R, Viereck V (2010) Tape functionality: position, change in shape, and outcome after TVT procedure—midterm results. Int Urogynecol J 21(7):795–800
26. Brandão FSQdS, Parente MPL, Rocha PAGG, Saraiva MTdQeCdM, Ramos IMAP, Natal Jorge RM (2015) Modeling the contraction of the pelvic floor muscles. Comput Methods Biomech Biomed Eng 1–10. doi:10.1080/10255842.2015.1028031
27. Peng Y, He J, Khavari R, Boone T, Zhang Y (2015) PD24-03 identification of innervation zones of the pelvic floor muscle from noninvasive high-density intra-vaginal/rectal surface EMG recordings. J Urol 4(193):e491
28. Liu Y, Ning Y, Li S, Zhou P, Rymer WZ, Zhang Y (2015) Three-dimensional innervation zone imaging from multi-channel surface EMG recordings. Int J Neural Syst 25(06):1550024
29. Yang L, Yong N, Jinbao H, Sheng L, Ping Z, Yingchun Z (2014) Internal muscle activity imaging from multi-channel surface EMG recordings: a validation study. In: Engineering in Medicine and Biology Society (EMBC), 2014 36th Annual International Conference of the IEEE, 26–30 Aug. 2014, pp 3559–3561. doi:10.1109/EMBC.2014.6944391
30. Yong N, Xiangjun Z, Shanan Z, Yingchun Z (2015) Surface EMG decomposition based on K-means clustering and convolution kernel compensation. Biomed Health Inform IEEE J 19(2):471–477. doi:10.1109/JBHI.2014.2328497